IEEE Access
Multidisciplinary | Rapid Review | Open Access Journal

Received February 3, 2021, accepted February 21, 2021, date of publication March 8, 2021, date of current version March 17, 2021.

Digital Object Identifier 10.1109/ACCESS.2021.3064462

An Extensive Study on the Performance Evaluation and Scheduling of HeNBs

RUI R. PAULO, (Member, IEEE), AND FERNANDO J. VELEZ, (Senior Member, IEEE)
DEM, Faculdade de Engenharia, Instituto de Telecomunicações and Universidade da Beira Interior, 6201-001 Covilhã, Portugal

Corresponding author: Rui R. Paulo (rrp@lx.it.pt)

This work was supported by Foundation for Science and Technology/Ministry of Science, Technology and Higher Education (FCT/MCTES) through national funds and, when applicable, co-funded EU funds under the project UIDB/50008/2020, COST CA 15104 Inclusive Radio Communication Networks for 5G and Beyond (IRACON), Optical Radio Convergence Infrastructure for Communications and Power Delivering (ORCIP, 22141-01/SAICT/2016), TeamUp5G and CONQUEST (CMU/ECE/0030/2017). The TeamUp5G project has received funding from the European Union's Horizon 2020 research and innovation programme under the Marie Skłodowska-Curie project number 813391.

ABSTRACT Since the dawn of mobile communication systems, reducing the cell size has been one option to increase the signal-to-interference-plus-noise ratio (SINR) in both links. The impact of this reduction can be perfectly understood by considering Shannon's law. This work studies in detail the performance of Home eNBs (HeNBs), nodes with a smaller coverage area. After a detailed theoretical study of the SINR, a simulation approach is used to extract performance results in small cell indoor scenarios. Results corresponding to the goodput, delay and packet loss ratio are analyzed. Based on an improved version of LTE-Sim, the proportional fair, frame level scheduler (FLS) and exponential rule are tested in an indoor environment. With the saturation conditions taken into consideration, the FLS performs better than the other schedulers. This work shows that with the considered applications, it is possible to achieve a reduction in the transmitter power of HeNBs without compromising the small cell network performance.

INDEX TERMS Delay, small cell, femtocells, goodput, HeNBs, LTE-Sim, packet loss ratio, packet scheduler, saturation conditions, SINR.

I. INTRODUCTION

Cellular networks began with the deployment of radio base stations with wide coverage areas. Those radio base stations have evolved into the currently used equipment, known as evolved Node Bs (eNBs), which are well modeled and tested (including drive tests) before they go to market. Presently, the trend in the mobile communications sector toward 5G is to have increasingly smaller cell sizes [1]. This reduction in the cell coverage area clearly enables the capacity to increase. Short range enables enhancement of the carrier-to-interference ratio while improving the system capacity and service quality [2]. This improvement due to the reduction in cell size can be explained by considering Shannon's law [3].

Currently, 80% of traffic occurs indoors, but most cellular networks are composed of outdoor eNBs. To respond to the increase in demand, e.g., at hotspots, in-building coverage has become a challenge [4]. Applications are also requiring more and higher throughputs [5]. The authors of [6] identify video streaming as the application with the highest throughput requirement. Moreover, in the future, ultra-high-definition videos with virtual reality [7] will require a significant long-term demand for bandwidth. In the longer-term forecasts of [7], the consumer segment will have 74% of its total devices connected to the network. Machine-to-machine (M2M) nodes, the fastest growing mobile segment, will comprise half the global connected devices. In fact, M2M applied to home environments includes applications such as video surveillance, smart meters, and healthcare monitoring, among an infinite number of possibilities. The consumption of video streaming, the increase in the number of M2M devices that include video among their capabilities, and the impact of video devices on mobile network traffic justify the need for studying video performance in mobile networks. In addition, mobile and M2M also generate several types of traffic flow with different traffic requirements, from video applications with a maximum delay of 150 ms to applications where the requirements for delay are not very critical (e.g., home environmental monitoring) [8]–[10].

When high-data-rate indoor coverage is provided by outdoor eNBs, if high-order modulation and coding schemes, e.g., 64/128/256 QAM, are used, the (external) walls of a building constitute an obstacle that is difficult to overcome or is impassable, creating indoor areas with weak or no signal

The associate editor coordinating the review of this manuscript and approving it for publication was Wenjie Feng.

coverage. Another approach to increase system capacity in 5G is to adopt high frequencies. However, higher frequencies will lead to a problem similar to that when considering high-order modulation and coding schemes, as they also create indoor areas with weak or even no signal coverage at all.

One solution to solve the lack of indoor coverage is to resort to smaller eNB coverage areas [11]. However, this solution does not solve all the identified issues, since it does not eliminate the physical barriers between eNBs and the destination nodes (usually known as user equipment, UE), e.g., walls or urban obstacles. Efforts to achieve higher capacities have led to the development of small cells, such as picocells or femtocells. Home eNBs (HeNBs) are some of the smallest cellular nodes and provide radio coverage within these femtocells. HeNBs deal with indoor coverage in areas where resorting to the traditional eNB coverage zones is not effective at all [12]. HeNBs are defined in [13] as small, inexpensive, low-power indoor base stations that are generally consumer deployed. This possibility of consumer-deployed HeNBs and the variety of preceding cell types with irregular sizes result in totally chaotic and random coverage shapes [13]. HeNBs are deployed not only in private houses but also in scenarios such as offices, shopping centers and industrial environments [14], [15]. In this case, HeNBs are known as Enterprise HeNBs.

The nature of the uncoordinated and disordered deployment of HeNBs contends with the existing network. This kind of deployment yields new and more complex interference problems in both downlinks and uplinks [2]. To solve these problems, power control [16]–[19] and new scheduling algorithms [20], [21] have been the main solutions proposed to mitigate the underlying interference problems while improving the operation of HeNBs. Due to the uncoordinated deployment nature of HeNBs, algorithms for interference-positioning are being developed as proposed by the authors of [22].

Different simulation approaches for the deployment of HeNBs followed by the research community [11], [23]–[27] consider the assumptions and parameters of [28].

In this work, the definition of the scenario follows some of the assumptions of the Technical Specification Group (TSG) Radio Access Network (RAN) from 3GPP [28]. A dense HeNB deployment model is adopted by considering a single-floor building composed of 25 apartments. These apartments have a square geometry and are placed next to each other on a 5×5 grid, resulting in a building also with a square geometry, as shown in Fig. 1.

Deploying buildings within macrocells yields the general behavior that incorporates the effects of taking HeNBs and served users at various distances from the eNB [29]. The deployment ratio determines whether HeNBs are deployed or not in all apartments. It varies from zero to one. If the deployment ratio is one, every apartment has an HeNB serving its UE. This assumption puts high pressure into the system since usually, as in [28], the deployment ratio is 0.2. This work considers a deployment ratio of one. HeNBs are deployed in the middle of the apartments. Although the optimal position is not studied in this work, the optimal position is in the middle of the apartments, as concluded by the authors of [30].

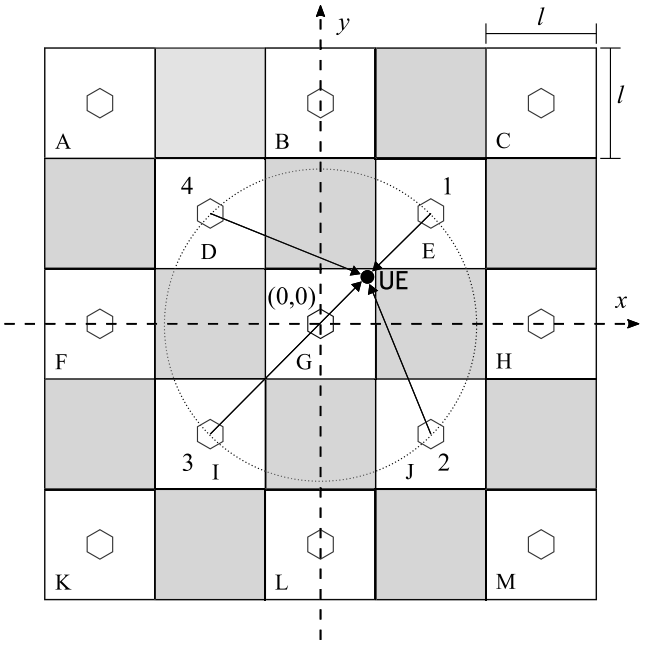

FIGURE 1. Simulation scenario of 25 apartments with reuse pattern 2.

In [22], the hypothesis of having illegitimate HeNBs that could damage the HeNB communication is studied. These illegitimate HeNBs acts as interferers. Frequency reuse is assumed in many works as a way to deal with co-channel interference and to enhance system performance. In the considered scenario, the HeNBs operate with a frequency reuse pattern of two. This assumption implies that in the considered deployment of this work, HeNBs with the same frequency act as illegitimate HeNBs (to the neighboring HeNBs), as studied in [22]. One assumes that eNBs operate with a frequency reuse pattern of one.

This study considers the variation in the transmitter power from HeNBs and in the side of apartments within a reasonable range. In [28], an interval for the available transmitter power of HeNBs is considered. The reduction in transmitter power considered in this study may lead to a reduction in interference. In [31], it is also stated that a reduction in the transmitter power can also reduce the coverage. Our study analyzes the variation in transmitter power in the HeNB layer without compromising the coverage.

These independent and noncorrelated variations increase the complexity of the theoretical study and provide a broader vision for the average signal-to-interference-plus-noise ratio (SINR) and its impact on system performance. In addition to the theoretical study, the goal is to evaluate the performance through simulation by considering LTE-Sim [32] with the extension of the works presented in [27], [33]. LTE-Sim is an open-source framework used to simulate LTE-Advanced networks, which has a high degree of reproducibility of the results.

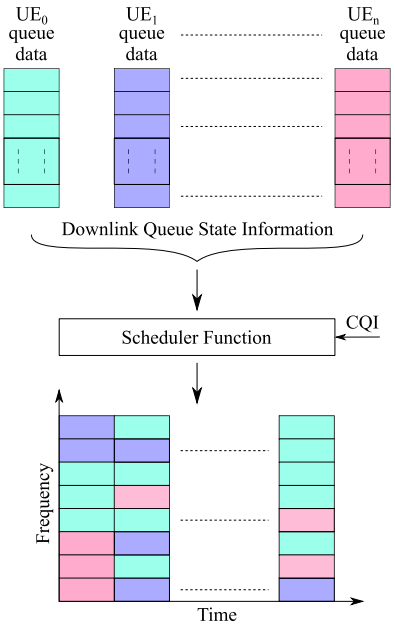

FIGURE 2. Simplified generic view of a wideband resource scheduler. Adapted from [36].

User traffic is supported by HeNBs, which continuously exchange data with them. The considered applications are video and best effort. Different from [34], [35], where a new scheduling algorithm was developed and/or a new bandwidth aggregation scheme was implemented to minimize the energy consumption, we explore the possibility of reducing the transmitter power of HeNBs without compromising the overall system performance.

The packet scheduler in the HeNB distributes the available radio resources among the UE. The details on the scheduling algorithms are left to the HeNB implementation. Fig. 2 shows a generic function of the downlink scheduler. Data are scheduled to a number of users on a shared set of physical resources. Packet schedulers can make scheduling decisions based on the channel quality indicator (CQI). The CQI is determined at the UE and then transmitted to the eNB via feedback signaling channels. Feedback is an important measurement since this information helps to maximize the data rate [36]. With this information, the scheduler at the eNB/HeNB must manage the data requirements of the UE under its control. These requirements exist to ensure that transmissions meet the desired service quality.

Performance evaluation of the packet scheduling in LTE networks involves studying the trade-off between the goodput, packet loss ratio (PLR) and delay. For the considered application mixture (video and best effort), the proportional fair scheduler, frame level scheduler and exponential rule scheduler are considered in the simulations while seeking system saturation. It is worth studying these schedulers since for 5G, there is still freedom in the choice to be considered [37]. In [37], some minor revisions in some schedulers (such as the proportional fair (PF) considered in this work) that allow them to support packet scheduling in the downlink OFDMA-based 5G networks are also presented. A comparison of the different schedulers facilitates the identification of their limitations and advantages in typical indoor deployment scenarios [38], [39]. System saturation is achieved by gradually increasing the number of users in each HeNB in an equitable way. Contrary to the simulation works from [5], [40]–[42], our study considers a higher number of users per HeNB, which implies a very large density of users within a building.

This work is in some way complementary to other simulation works, such as [4], [43], [44], since it presents a higher number of deployed HeNBs and a path loss model that considers and counts the number of walls between users and HeNBs. For simulation purposes, although fewer schedulers are considered for the simulation than in [43] and changes to existing schedulers are not considered as in [44], in this work, an in-depth determination of the variation in the number of supported users in saturation conditions, as a function of the apartment side length and the transmitter power is carried out with narrower confidence intervals.

The remainder of the article is organized as follows. The average SINR is analytically studied in Sec. II. Sec. III presents the simulation scenario and physical settings and addresses the performance evaluation of small cells. Different packet schedulers are considered. The simulations results are presented in Sec. IV. Finally, conclusions are drawn in Sec. V.

II. STUDY OF THE AVERAGE SINR

A. SCENARIO

In this work, we consider a single-floor building with 25 apartments, as shown in Fig. 1. Apartments are placed next to each other in a 5 × 5 grid geometry. HeNBs operate with a 10 MHz bandwidth and a frequency reuse of two [36], [45], i.e., the total 20 MHz of available bandwidth is divided into two equal parts of 10 MHz. The impact of considering a 20 MHz or 10 MHz bandwidth and the mapping of the SINR into the maximum supported throughput are presented in [46] and [47]. The HeNBs in the apartments, represented by the light gray fill in Fig. 1, use the 10 MHz bandwidth, while the apartments with white fill use the remaining 10 MHz. In Fig. 1, the HeNBs are represented by a hexagonal shape. Although there is one HeNB inside each apartment, only HeNBs in the apartments with white fill are represented.

Following the approach implemented by us in [33], users are truly located inside their own apartments. This means that there are no walls between a user and the corresponding HeNB. When the user is served by a HeNB using a given frequency band, it will suffer interference from the co-channel HeNBs. Since a reuse pattern of two is considered, there will be three different cases of interference for the first tier of interference from the HeNBs to the user terminals. In the first case, the users are inside apartments D, E, G, I, and J, and there are four neighboring interferers close to their apartments, as shown in Fig. 1. In the second case, the users are inside apartments B, F, H, and L, and there are only two

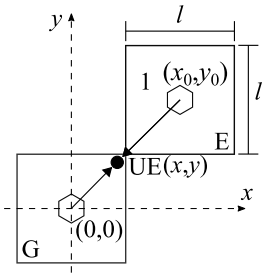

FIGURE 3. Interference received from one of the neighboring HeNBs and the signal from the user's own HeNB.

neighboring interferer HeNBs. In the third case, the users are inside apartments A, C, K, and M, and there is only one neighboring interferer.

B. SINR AT A GIVEN POSITION

For the sake of simplicity, let us consider the central apartment G and apartment E, which causes interference to users from apartment G, as shown in Fig. 1. Let us assume a user equipment/terminal, in our case, user equipment (UE), inside and confined to apartment G of the considered topology, as shown in Fig. 3.

The center of the apartment is also the origin of the coordinate system (0, 0). To obtain the average SINR, an approach similar to the one described in [11], [48], [49] is applied. In general, the SINR from the considered UE, at a position with the coordinates (x, y), served by a cell with a transmitter power P_{Tx} (in linear terms) can be expressed as

$$\mathrm{SINR}(P_{Tx}, x, y) = \frac{P_{ow}(P_{Tx}, x, y)}{(1-\alpha)\cdot P_{ow}(P_{Tx}, x, y) + P_{nh}(P_{Tx}, x, y) + P_{noise}}, \quad (1)$$

where P_{ow} is the average amount of power received from the user's own cell and α is the orthogonality factor of the codes [50]. For the sake of simplicity, and according to [51], α is considered to be equal to one. P_{nh} is the average interference power from the neighboring cells. P_{noise} is the thermal noise power. In (1), all these powers are given in linear terms. P_{noise}, in dBW, is defined as follows:

$$P_{noise} = -174 + 10 * \log_{10} BW - 30 + NF, \quad (2)$$

where NF is considered to be 8 dB (for LTE, NF is typically 7-9 dB [28]) and the bandwidth $BW = 10$ MHz.

The average interference generated by a neighboring cell can be calculated by integrating each fraction of the interference power over the area of the affected cell. Fig. 3 shows a cell affected by interference at the origin of the coordinates and one interfering cell at (x_0, y_0). By integrating over the cell area, the average level of the power received from a neighboring cell, $\bar{I}$, may be calculated as

$$\bar{I} = \int_x \int_y f_I(P_{Tx}, x, y)dxdy = \int_x \int_y \frac{P_{Tx}G_{Tx}G_{Rx}}{A_{Apt}} PL(x, y)dxdy, \quad (3)$$

where G_{Tx} and G_{Rx} are the transmitter and receiver gains, respectively. A_{Apt} is the total affected apartment area.

Although the path loss model recommended in [28] avoids modeling any walls, the WINNER II path loss model [52] adopted in this work considers the number of walls located in between the user and the HeNBs. For an indoor office, the path loss equation of the WINNER II model is as follows:

$$PL_{HeNB}(x, y) = A * \log_{10}(d) + B + C * \log_{10}(\frac{f_c}{5}) + X, \quad (4)$$

where d is the distance between the transmitter and the receiver, f_c is the frequency in GHz, and the fitting parameter A includes the path loss exponent. Parameter B is the intercept, parameter C describes the path loss frequency dependence, and X is an environment-specific term (e.g., wall attenuation in the non-line-of-sight (NLoS) scenario [52]). The distance d is determined by the Euclidean distance:

$$d = \sqrt{(x - x_0)^2 + (y - y_0)^2}, \quad (5)$$

where x_0 and y_0 are the coordinates of the interfering cell and x and y are the coordinates of the UE, as shown in Fig. 3; in this study, $f_c = 2$ GHz. For line-of-sight (LoS) propagation, $A = 18.7$, $B = 46.8$, and $C = 20$. In the NLoS case, $A = 20$, $B = 46.4$ and $C = 20$. The environment-specific term X is the sum of the attenuation of the walls between the UE and HeNB. For internal walls, the attenuation is 5 dB.

In the first case, the central HeNB is considered, and there are four HeNBs in the first ring of interference (labeled 1, 2, 3 and 4), as shown in Fig. 1. Considering only the interferer HeNB from Fig. 3 (identified by number 1), the path loss is given by the following equation:

$$PL(x, y)_1 = 20 * \log_{10}(\sqrt{(x - l)^2 + (y - l)^2}) + 46.4 + 20 * \log_{10}(\frac{2}{5}) + 2 * 5, \quad (6)$$

where l is the apartment side length. For the remaining three HeNBs in the first ring of interference (2, 3 and 4 in Fig. 1), the coordinates (x_0, y_0) change to $(l, -l)$, $(-l, -l)$ and $(-l, l)$, respectively, as shown in Fig. 1. In this first case, only four interferers are assumed, as due to the increase in the number of walls and the longest distance between HeNBs from the farthest ring of interference and the user, the underlying share of interference is negligible.

For the second and third cases, in addition to the change in the number of interferer HeNBs, as explained above, the change in coordinates of the user's own cell and of the interferers need to be considered. In the second case, there are only two interferers in the first ring of interference, while in the third case, there is only one interferer.

C. AVERAGE SINR

UE is uniformly distributed over the apartment area. According to [51], the average SINR experienced by UE depends on the apartment side length l and on the HeNB transmitter

power, P_{Tx}, as follows [53]:

$$\overline{\text{SINR}}(l, P_{Tx}) = \frac{\bar{P}_{ow}(l, P_{Tx})}{\bar{P}_{nh}(l, P_{Tx}) + P_{noise}}. \quad (7)$$

The average interference power $\overline{P}_{nh}$ can be defined as

$$\overline{P}_{nh}(l, P_{Tx}) = \sum^{n_T} \bar{I}(l, P_{Tx}), \quad (8)$$

which is the total surrounding power received from interfering neighbors at different distances. The average interference generated by the interfering HeNBs can be calculated by integrating each fraction of the interfering power over the affected area. Since the UE is confined to the apartment area, the average level of received interference from a neighboring cell $\bar{I}$ is integrated over the apartment area:

$$\begin{aligned}\bar{I}_i(l, P_{Tx}) &= \sum_{i=1}^{n_T} \int_{\Gamma_x^i} \int_{\Gamma_y^i} f_{I_i}(P_{Tx}, x, y) dydx \\ &= \sum_{i=1}^{n_T} \int_{\Gamma_x^i} \int_{\Gamma_y^i} \frac{P_{Tx} G_{Tx} G_{Rx}}{A_{Apt}} PL(x, y) dxdy. \quad (9)\end{aligned}$$

The integration regions for an interferer HeNB are as follows:

$$\Gamma_x^i = \{[-l/2, l/2]\} \quad (10)$$

and

$$\Gamma_y^i = \{[-l/2, l/2]\}. \quad (11)$$

According to [54], the following parameters are considered: $G_{Tx} = 5$ dBi and $G_{Rx} = 0$ dBi.

The average power received from the user's own cell, $\overline{P}_{ow}(P_{Tx,x,y})$, is constant no matter the value of the reuse pattern. It may be obtained by following an approach similar to the one used in the computation of $\overline{P}_{nh}(l, P_{Tx})$ but with a different integrand function:

$$\begin{aligned}\overline{P}_{ow}(l, P_{Tx}) = \int_y \int_x & \frac{P_{Tx} G_{Tx} G_{Rx}}{A_{ow}} \\ & 10^{-\frac{18.7 * \log_{10}(\sqrt{(x^2+y^2)}) + 46.8 + 20 * \log_{10}(\frac{2}{5})}{10}} dxdy. \quad (12)\end{aligned}$$

However, the integration area includes the origin of the coordinate system, $(x, y) = (0, 0)$. Since the HeNB is at those coordinates [55], equation (12) converges to infinity and is unsolvable. Without considering a circular area with a radius equal the Fraunhofer distance, F_r, the circle with the white fill in Fig. 4, extracted from the total cell area (12), becomes solvable. A_{ow} is the total integration area, represented by the gray fill in Fig. 4:

$$A_{ow} = l^2 - \pi \times F_r^2. \quad (13)$$

The integration limits of (12) take into consideration subtraction of the circular area with a radius equal the Fraunhofer distance.

Fig. 5 presents the results for the average SINR as a function of the apartment side length, l, and the transmitter power, P_{Tx}. The apartment side length varies from 5 to 35 m, while the transmitter power varies from −20 to 30 dBm.

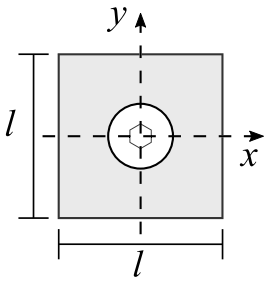

FIGURE 4. Circular apartment area with a radius equal the Fraunhofer distance.

Fig. 5a shows that the variation in transmitter power for the same apartment side length does affect the average SINR results for the first case. For the second and third cases, as the number of interferers decreases, the average SINR increases, as shown in Figs. 5b and 5c. However, when the apartment side length increases and the transmitter power decreases, the signal strength is not enough to provide an increase in the average SINR. This effect is clearer when the apartment side length is 35 m and transmitter power is −20 dBm.

III. PERFORMANCE EVALUATION

We study the system performance for the downlink (DL) by considering the parameters and assumptions discussed below. The simulations consider LTE-Sim, in its stable release R5 [32], to investigate the overall system performance.

A. SIMULATION SCENARIOS AND PARAMETERS

LTE-Sim is an event-driven simulator that was written in C++ using the object-oriented paradigm [32]. In its stable release R5, it is compiled with an ISO/IEC 14882:1998 compiler. With this compiler, the underlying random number generator may not be uniformly distributed.

In [11], the authors solved this by taking advantage of the Mersenne Twister pseudorandom generator [56]. The Mersenne Twister is the most widely used general-purpose pseudorandom number generator [57] and was made available in ISO/IEC 9899:2011 [58]. To correctly start the Mersenne Twister pseudorandom number generator, the seeds consider the time library Chrono. This library is also available in ISO/IEC 9899:2011 [58].

To address the behavior in a real scenario through event-based simulation while conserving computational resources, the simulation scenario is composed of an eNB with a 1 km radius (represented by the solid line circle in Fig. 6).

The deployment of the building with 25 apartments in the eNB coverage area makes up a realistic scenario [59]. We created a one-floor building with a 5 × 5 grid geometry, with 25 apartments in an area with a radius 80 % of the macrocell radius (represented by the dashed line in Fig. 6). This constraint ensures that buildings do not cross the macrocell edge. Although the reduction in coverage cell area improves the system capacity, eNBs cannot be decommissioned since they play a key role in providing wide cell coverage, especially in outdoor scenarios, such as streets, roads and suburban areas.

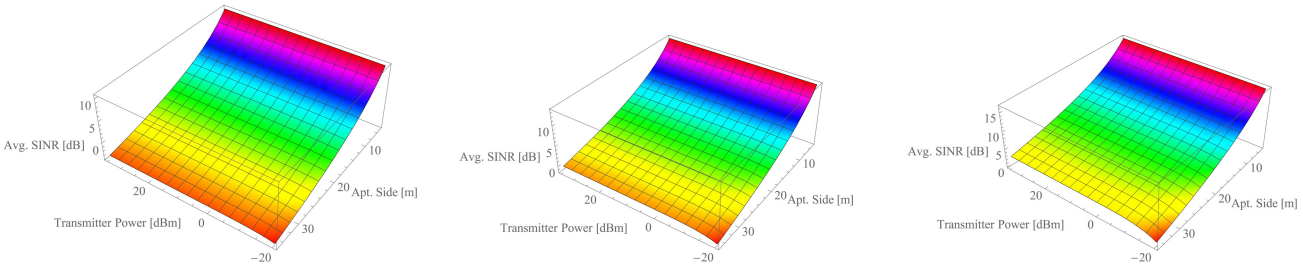

(a) First Case (b) Second Case (c) Third Case

FIGURE 5. Average SINR for an apartment side length from 5 to 35 m and a transmitter power from −20 to 30 dBm. The first case has four interferers, the second case has two interferers, and the third case has one interferer.

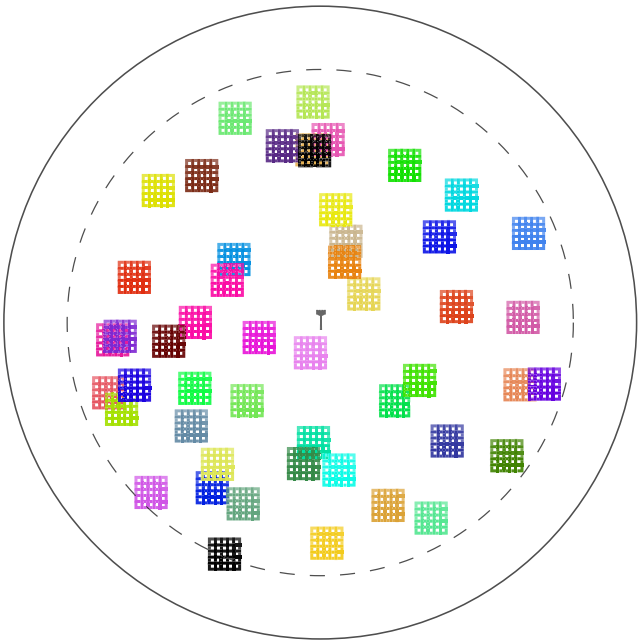

FIGURE 6. The fifty different positions of the building are randomly chosen.

In 2003/04, we deployed WLANs in the Department of Electromechanical Engineering at the University da Beira Interior and Hospital Universitário Pêro da Covilhã, Portugal. During the site survey we performed prior to access point deployment, we concluded that relevant interference between two adjacent floors occurs only in the room immediately below or above the zone where the node is deployed. Hence, in similar way, if a small cell network is deployed on the next floor, the frequency reuse problem is solved, with the frequency channels shifted by one room [60], [61].

In the old versions of LTE-Sim, most of the buildings and users over a circular-shaped macrocell were close to the center. Hence, they were not truly uniformly distributed over the macro-cellular area. This limitation required improvement. The simulator considers Cartesian coordinates generated from polar coordinates. To overcome the identified limitations and achieve a uniform random distribution of the users or buildings within the circular area that represents the macrocell, the simulator obtains the radial distance by multiplying the radius by the square root of a uniform random number between zero and one. As previously explained, for buildings, this radius is 80% of the cell radius. Moreover, the angular coordinate is uniformly distributed between zero and 360 degrees. The results presented below already benefit from these improvements made to the simulator.

There is one HeNB at the center of each apartment [26], [28]. This geometry represents home, office and shopping center actual deployment scenarios. The considered values for the transmitter power in the HeNBs are 0 dBm, 10 dBm, and 20 dBm. All cells simultaneously operate at the same power level. In terms of apartment dimensions, in [28], only an apartment side length of 10 m is considered. In this work, the side length of the apartments (identified as Side in the figures) varies from 5 m to 20 m in steps of 5 m. The maximum number of users per HeNB considered in [28] is four, but the results from [27], [33] show that the maximum system capacity in the considered scenarios was not achieved. This result allowed for exploring the existence of more users per HeNB.

Since LTE-Sim considers the generation of users in HeNBs, taking into account the influence area of each HeNB, this coverage influence area of the HeNB is a circle. The authors of [33] considered the users to be inside the apartment and the apartments to be bounded by a square. The distribution of users in this square area was also updated by the authors by considering the Mersenne Twister pseudorandom number generator in addition to the WINNER II [52] path loss model. This model was not considered by 3GPP in [28]. More details are presented in Tab. 1.

We considered a heterogeneous scenario with a mixture of two different applications. One is video, while the other is best effort (BE). Video is an application with a guaranteed bit rate, while the BE type of resources has a non-guaranteed bit rate [37]. We tested the network performance by considering the video and BE flows. The video application is represented by a video trace that is compressed using the H.264 standard compression at the average coding rate of 440 kb/s, available in [62]. The adoption of this video application accounts for the trend of users to watch high-quality videos. The BE application models an ideal greedy source that always has packets to send. BE transmits packets only when there are enough resources to send them. A maximum of 100 ms is considered for the delay. The maximum delay is the maximum tolerable time interval within which each packet must be received. When this maximum delay is surpassed, the

TABLE 1. Simulation parameters.

Parameters	
Simulation duration	30 s
Flow duration	20 s
Frame structure	FDD
CQI	Periodic
Number of eNBs	1
eNB cell radius	1 km
eNB cluster	1
eNB bandwidth	20 MHz
Number of HeNBs	25
HeNB cluster	2
HeNB bandwidth	10 MHz + 10 MHz
Access policy	Open
Power of HeNBs	[0, 10, 20] dBm
Initial number of users per HeNB	6
User speed	0 km/h
User position	Random
Application type	Video and best effort
Video bit rate	440 kb/s
Maximum delay	0.1 s
Number of buildings	1
Number of floors	1
Geometry of buildings	5x5
Apartment side length	[5, 10, 15, 20] m
Building position	Random
Path loss model	WINNER II
Number of simulations	50

packet is dropped. The considered channel quality indicator (CQI) feedback is considered periodic. Within the CQI reporting feature, the UE estimates the channel quality and converts it into a set of CQI feedbacks reported periodically to the HeNB. This version of the simulator, which includes the improvements from this work, is freely available under the GPLv3 license [63].

B. PACKET SCHEDULERS

To analyze the overall performance of the system in the downlink (DL), we considered three packet schedulers [32]: proportional fair (PF), frame level scheduler (FLS) and exponential rule (EXPRule). These schedulers are available in LTE-SIM. According to [38], [39], [43], [44], they are channel sensitive, i.e., UE intermittently forwards a CQI report to the HeNB. This CQI report presents the channel quality experienced by each UE and estimated by the scheduler. PF and EXPRule are schedulers that are unaware of the service type. In the opposite way, the FLS divides flows in both real time and non-real time. In this work, one of the studied parameters is the maximum average delay per video. From the considered schedulers, the FLS and EXPRule are the ones that consider delay-aware strategies. This type of approach is the most suitable for the considered video application. In terms of quality service, PF is a scheduler with an approach unaware of the service type [43], [44].

1) PROPORTIONAL FAIR

PF schedules a user when its instantaneous channel quality is high relative to its own average channel condition over time [36]. The PF scheduler seeks a trade-off between fairness and spectral efficiency [64] but is somehow limited in terms of spectral efficiency [38]. It is effective in reducing variations in user bit rates with little average bit rate degradation as long as the user average values of the SINR are fairly uniform [65].

2) FRAME LEVEL SCHEDULER

In the approach presented in [39], time is seen as an endless sequence of frames, which are further split into time intervals. At the highest level, the FLS is an innovative low-complexity resource allocation algorithm that was designed using discrete time linear control theory. At the beginning of each frame, the FLS computes the amount of data that each real-time source should transmit within the frame to satisfy its delay constraint. Then, to ensure fairness among multimedia flows, the lowest-level scheduler assigns radio resources according to the PF algorithm [66] subject to the constraint imposed by the FLS.

3) EXPONENTIAL RULE

In [67], the EXPRule was studied as a scheduling algorithm that explicitly uses information on the state of the channel and queues. The authors mention, as a main result, that the EXPRule throughput is optimal, i.e., it renders queues stable in any system for which stability is feasible at all, with any other rule. Although the complexity of this scheduler is high [38], the EXPRule and Logarithmic Rule have been presented as the most promising approaches for DL scheduling in LTE systems with delay-sensitive applications [68].

For each scheduler and for each combination of values of the HeNB transmitter power and apartment side length, we performed fifty simulations. In Fig. 6, fifty unique positions of the buildings are simultaneously shown. The goal of accounting for different positions is to acquire the general behavior that integrates the contribution of the effect of having the building, and consequently the HeNBs and the served users, at different distances from the eNB. We evaluated the network performance in terms of the goodput, packet loss ratio (PLR), and delay of video and the goodput achieved by BE flows.

IV. SIMULATION RESULTS

Simulations have been performed in LTE-Sim to obtain the variation in not only the packet loss ratio (PLR), goodput and delay for a video application but also the goodput for the best BE application. We have also performed a detailed comparison of the performance of the considered packet schedulers.

A. PACKET LOSS RATIO FOR VIDEO

The packet loss ratio is the ratio between the total number of packets that fail to reach their destination and the total number of transmitted packets. In this section, the video

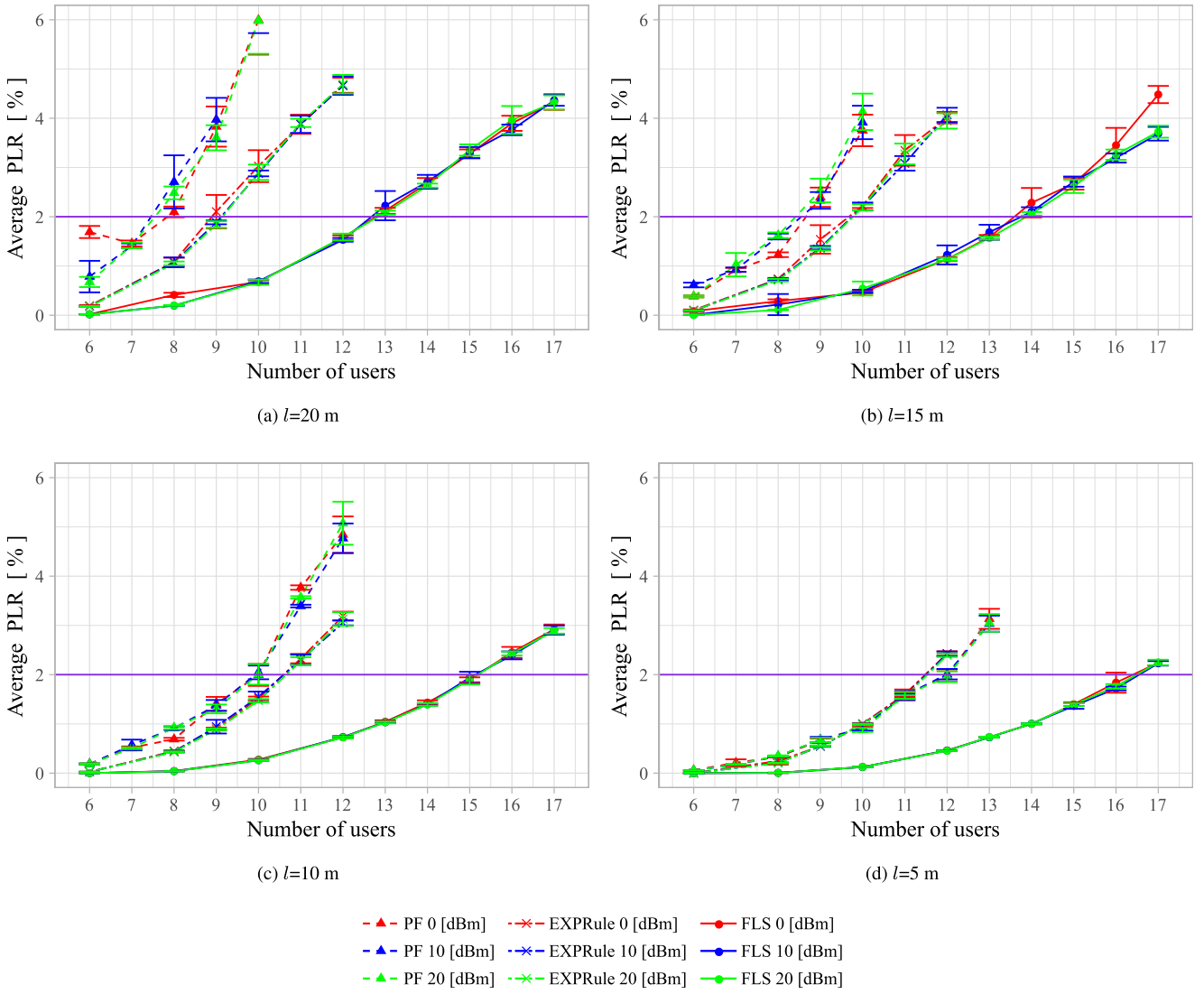

FIGURE 7. Average packet loss ratio as a function of the number of video users for different apartment side lengths and transmitter powers.

application is considered. Fig. 7 presents the results for the average PLR as a function of the number of users for all the considered scenarios. The values of the transmitter power are 0, 10 and 20 dBm. The considered apartment side lengths are 20, 15, 10 and 5 m.

In the simulations, for all combinations of the apartment side length, transmitter power and scheduler, the number of users spans between 6 users per HeNB and the number of users that corresponds to surpassing the PLR threshold of 2%. According to [69], the PLR threshold for video is 2% or, more precisely, PLR<2%. The results are presented in [4], [44], where the users determine their quality of experience by analyzing video transmissions expressed by the mean opinion score (MOS). A literature review indicates that for values of the PLR higher than 2%, the MOS decays, resulting in an uncomfortable video user experience and yielding a PLR threshold of 2%.

For the three schedulers, the average PLR increases with the number of users. Furthermore, it is a worth comparing the results by distinguishing two cases:

- apartment side lengths of 20, 15 and 10 m (Figs. 7a, 7b and 7c, respectively);
- apartment side length of 5 m (Fig. 7d).

For the first case, when the threshold is 2%, the PF (dashed line) scheduler supports fewer users than the EXPRule (double-dashed line) scheduler. The EXPRule also supports fewer users than the FLS (solid line).

For the second case, the EXPRule presents a higher average PLR than that of the PF. However, both schedulers continue to have worse results than those of the FLS. One can conclude that with this increase in apartment side length, all schedulers present a higher average PLR for video. Overall, the FLS performs better than the PF and EXPRule schedulers.

TABLE 2. Maximum number of users served by each scheduler for a PLR threshold of 2%.

Max. number of users		Transmitter power [dBm]								
		0			10			20		
		PF	EXPRule	FLS	PF	EXPRule	FLS	PF	EXPRule	FLS
Side length [m]	5	12	11	16	11	11	16	12	11	16
	10	10	10	15	9	10	15	9	10	15
	15	8	9	13	8	9	13	8	9	13
	20	7	8	12	7	9	12	7	9	12

B. MAXIMUM NUMBER OF SUPPORTED USERS

Tab. 2 summarizes the number of supported users for different side lengths of the apartments, values of the transmitter power and schedulers. We obtain these values for a PLR threshold of 2%.

For the FLS, i.e., the scheduler with the best performance, for an apartment side length of 5 m, the maximum number of supported users is 16 for all values of the transmitter power. For an apartment side length of 20 m, the FLS supports only 12 users.

For the EXPRule scheduler, for an apartment side length of 5 m, the maximum number of supported users is 11, while an apartment of 20 m supports 9 users (for a transmitter power of 10 and 20 dBm) or 8 users (for a transmitter power of 0 dBm).

For an apartment side length of 5 m, with the PF scheduler, the maximum number of supported users is 12 (for a transmitter power of 0 and 20 dBm) or 11 (for a transmitter power of 10 dBm), while for an apartment of 20 m, the PF scheduler supports only 7 users.

C. MAXIMUM AVERAGE GOODPUT FOR VIDEO

Considering an average PLR threshold of 2%, it is worthwhile to determine the maximum average goodput. We also compare the behavior of the maximum average goodput with the trend of the average SINR, as shown in Fig. 5.

When the apartment side length is 20 m or 15 m, the maximum average goodput is determined for video for the PF scheduler and all values of the transmitter power, as shown in Fig. 8. For other apartment side lengths, the average goodput is higher for a transmitter power of 0 dBm. For a side length of 5 m and a transmitter power of 20 dBm, the maximum values of the average goodput are the same as for a transmitter power of 0 dBm.

The maximum average goodput for EXPRule, from Fig. 9, has the same variations as those of the chart corresponding to the average SINR.

In general, along the same apartment side, the variation in the transmitter power does not affect the maximum average goodput. The exception occurs when combining an apartment side length of 20 m and a transmitter power of 0 dBm. Under these conditions, the EXPRule cannot sustain system performance. This behavior in the study of the average SINR occurs for the lowest values of the transmitter power and the longest apartment side lengths.

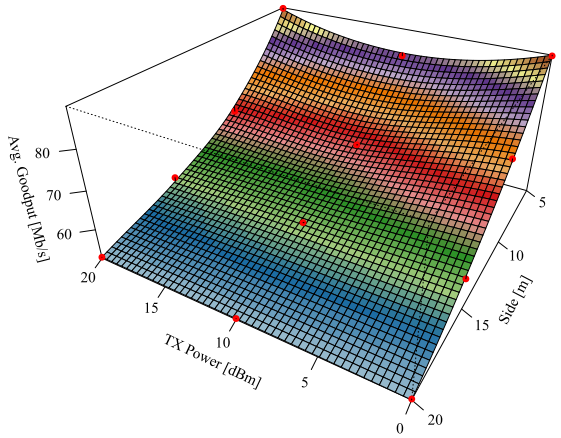

FIGURE 8. Maximum average goodput for video when the PF scheduler is considered.

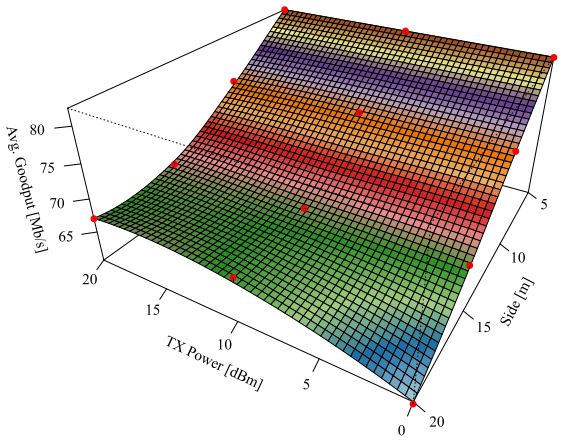

FIGURE 9. Maximum average goodput for video when the EXPRule scheduler is considered.

The FLS is the scheduler that supports more users. Varying the transmitter power along the same apartment sides has no impact, as shown in Fig. 10. The goodput for the FLS follows the same behavior as that of the average SINR.

For all schedulers, we observed a significant variation in the maximum average goodput along the apartment side. We obtained higher values for lower apartment side lengths, which agrees with the values and the lessons learned in Section II. Tab. 3 presents a summary of the maximum average goodput for each scheduler for video and BE applications.

D. MAXIMUM AVERAGE DELAY FOR VIDEO

We observe that the delay also increases when the number of users increases. The maximum delay for the PF scheduler

TABLE 3. Average goodput of video and BE applications for a PLR threshold of 2%.

Avg. goodput [Mb/s]	PF		EXPRule		FLS	
	Min.	Max.	Min.	Max.	Min.	Max.
Video	45.5	89	45.5	82	89	119
BE	310	390	315	400	285	361

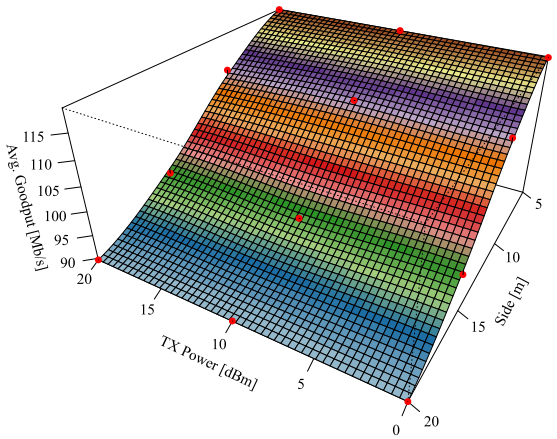

FIGURE 10. Maximum average goodput for video when the FLS is considered.

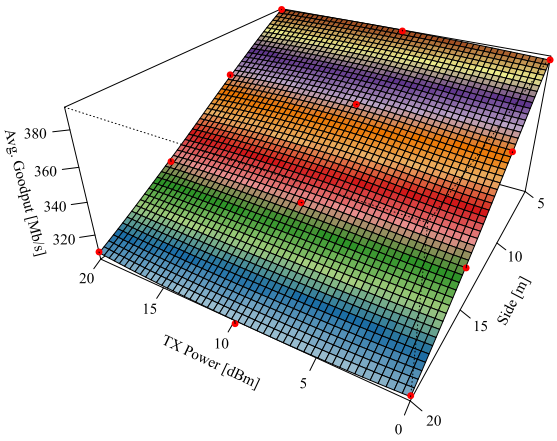

FIGURE 11. Maximum average goodput for BE when the PF scheduler is considered.

was 55 ms, for EXPRule was 25 ms and for the FLS was 28 ms. In none of the simulations did we exceed the maximum 3GPP limit of 150 ms for the maximum video delay.

E. MAXIMUM AVERAGE GOODPUT FOR BEST EFFORT

The best effort (BE) application makes use of the remaining resources left by the video application. Since the BE application sends packets only when there are enough resources to send them, the PLR is zero or near-zero. The few packets that do not reach their destination are lost because of the errors in the physical layer.

The maximum average goodput for BE is presented in Figs. 11, 12 and 13, respectively, for the PF, EXPRule and FLS. The EXPRule scheduler achieves the highest average goodput (400 Mb/s) among the three schedulers. The scheduler with the lowest maximum average goodput (285 Mb/s) is the FLS. More results for the maximum average goodput from BE are given in Tab. 3.

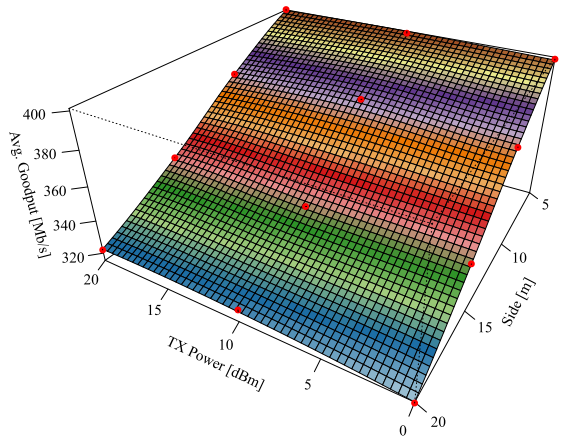

FIGURE 12. Maximum average goodput for BE when the EXPRule scheduler is considered.

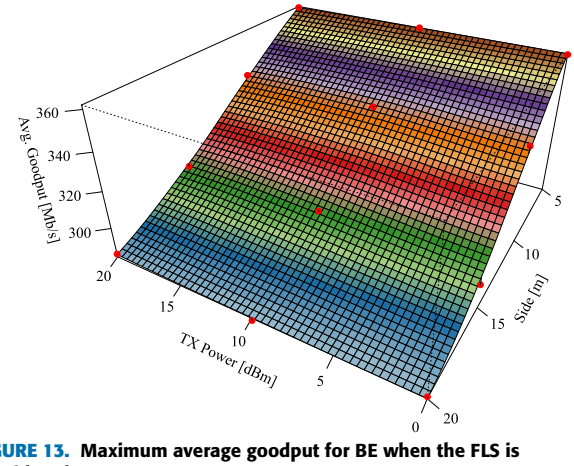

FIGURE 13. Maximum average goodput for BE when the FLS is considered.

The results are in line with the results from Section II. As opposed to the results obtained for the video application, the EXPRule scheduler presents the best performance for the BE application. The opposite occurs for the FLS.

It is straightforward to conclude that the behavior of all the packet schedulers when users are considering the BE application is identical. The goodput varies only when the apartment side length also varies. The maximum average goodput for BE retains the same behavior as that of the theoretical average SINR. The results show that the higher the maximum goodput for video is, the lower the maximum goodput for BE.

F. COMPARISON BETWEEN PACKET SCHEDULERS

To determine which packet scheduler has the best performance, we compare the results of the difference in the values

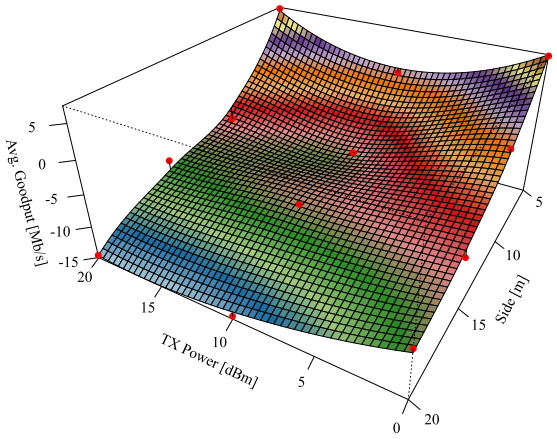

FIGURE 14. Comparison of the maximum average goodput for video between the PF and EXPRule schedulers.

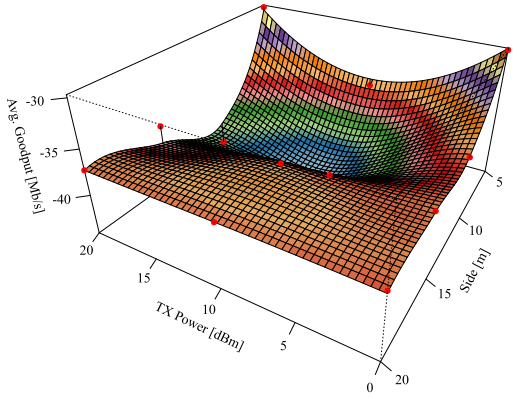

FIGURE 15. Comparison of the maximum average goodput for video between the PF scheduler and FLS.

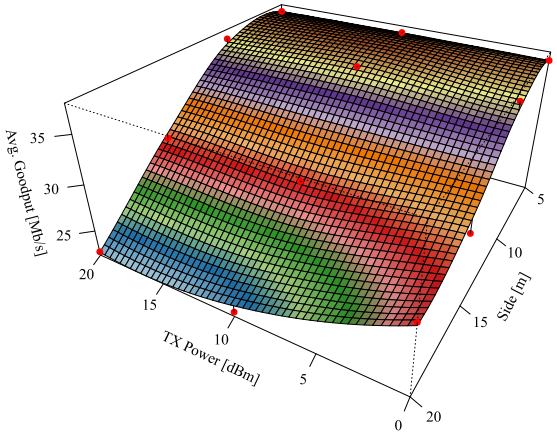

FIGURE 16. Comparison of the maximum average goodput for video between the FLS and EXPRule scheduler.

of the goodput between each pair of schedulers. Fig. 14 presents the difference in the goodput between PF and EXPRule. For apartments with a 5 m side length, the PF scheduler has the best performance. For other apartment side lengths, the EXPRule scheduler has the best performance.

Fig. 15 compares the goodput between the PF scheduler and FLS. The FLS has the best performance for any pair of values of the transmitter power and apartment side length. The FLS could, in the best case, operate with a goodput higher than 44 Mb/s compared to the PF scheduler.

In comparison to the EXPRule scheduler, the FLS shows once more its superior behavior, as shown in Fig. 16. The overall analysis shows that for the considered applications, the FLS performs better than the other two packet schedulers. In some combinations, the FLS performance is approximately 44 Mb/s higher than that of PF.

For small apartment sizes, PF is a better option than the EXPRule scheduler. For larger apartment sizes, the opposite is observed, and the EXPRule option prevails.

V. CONCLUSION

As most mobile communication traffic is shifting from outdoor to indoor environments, this work studied HeNBs (a particular case in the family of small cells) to offer indoor coverage. We considered a building with a 5×5 apartment topology. This work goes further than the assumptions of 3GPP by considering a higher-density deployment of HeNBs and users. This work also explored variations in the transmitter power of HeNBs and variation in the geometrical dimensions.

In the theoretical study of the average SINR, we identified three different cases for the first tier of interference. In the first case, a variation in transmitter power for the same apartment side length does not have any impact. For the second and the third cases, as the number of interferers decreases, the average SINR increases. However, when the apartment side length increases and the transmitter power decreases, the signal strength is not enough to attain an increase in the average SINR.

LTE-Sim was adopted to study the indoor 4G system under saturation conditions. The number of users served by each HeNB increased until the packet loss ratio surpassed the threshold value of 2% for video. For all considered combinations of the transmitter power and apartment side length, the maximum number of users appointed by 3GPP (i.e., 4) was largely surpassed by all schedulers.

The difference between the proportional fair (PF) and exponential rule (EXPRule) schedulers shows that for apartments with a 5 m side length, the PF scheduler has the best performance. For longer apartment side lengths, the EXPRule scheduler has the better performance. In comparison with PF, the frame level scheduler (FLS) has the best performance for any value of the transmitter power and apartment side length. The FLS also performs better than the EXPRule scheduler. For the considered video flow, the FLS presents the best overall performance. It enables service for up to sixteen users. For the video application, the results also show that it is possible to consider a reduction in the transmitter power without compromising the video performance.

The results for BE applications also show that it is possible to consider, in most cases, a reduction in the transmitter power. This reduction does not have a negative impact on system performance and can provide a reduction in energy consumption for both video and BE flows.

ACKNOWLEDGMENT

The authors thank Prof. Gastão Bettencourt from Centro de Matemática e Aplicações, Faculdade de Ciências, Universidade da Beira Interior, Portugal, and Prof. Giuseppe Piro from the Telematics Research Group, Politecnico di Bari, Italy, for their valuable contributions.

REFERENCES

[1] ArrayComm. (2011). *Cooper's Law*. [Online]. Available: http://www.arraycomm.com/technology/coopers-law/

[2] H. Zhang, C. Jiang, N. C. Beaulieu, X. Chu, X. Wen, and M. Tao, "Resource allocation in spectrum-sharing OFDMA femtocells with heterogeneous services," *IEEE Trans. Commun.*, vol. 62, no. 7, pp. 2366–2377, Jul. 2014.

[3] W. Webb, *Wireless Communications: The Future*. Hoboken, NJ, USA: Wiley, 2007.

[4] I. Rehman, M. Nasralla, and N. Philip, "Multilayer perceptron neural network-based QoS-aware, content-aware and device-aware QoE prediction model: A proposed prediction model for medical ultrasound streaming over small cell networks," *Electronics*, vol. 8, no. 2, p. 194, Feb. 2019. [Online]. Available: https://www.mdpi.com/2079-9292/8/2/194

[5] Z. Liu, W. Wang, K. Y. Chan, K. Ma, and X. Guan, "Rate maximization for hybrid access femtocell networks with outage constraints based on pricing incentive mechanism," *IEEE Trans. Veh. Technol.*, vol. 69, no. 6, pp. 6699–6708, Jun. 2020.

[6] C. W. Paper. (Feb. 2015). *Cisco Visual Networking Index: Global Mobile Data Traffic Forecast Update 2014–2019 White Paper*. [Online]. Available: http://www.cisco.com/

[7] Cisco. (Mar. 2020). *Cisco Annual Internet Report (2018–2023) White Paper*. [Online]. Available: https://www.cisco.com/c/en/us/solutions/collateral/executive-perspectiv%es/annual-internet-report/white-paper-c11-741490.pdf

[8] *Machine-to-Machine Communications (M2M); Definitions*, Standard ETSI, TR102 725 V1.1.1, ETSI, Jul. 2013.

[9] *Machine-to-Machine Communications (M2M); M2M Service Requirements*, Standard ETSI, TS 102 689 V2.1.1, Jul. 2013.

[10] *Machine-to-Machine Communications (M2M); Functional Architecture*, Standard ETSI, TS 102 690 V2.1.1, Oct. 2013.

[11] R. R. Paulo, F. J. Velez, and G. Piro, "Design of coordinated HeNB deployments," in *Proc. IEEE 87th Veh. Technol. Conf. (VTC Spring)*, Jun. 2018, pp. 1–6.

[12] M. R. K. Sial, H. F. Usman, and S. Hamid, "Green cognitive femtocells deployment house modelling for interference mitigation," in *Proc. 15th Int. Conf. Electr. Eng./Electron., Comput., Telecommun. Inf. Technol. (ECTI-CON)*, Jul. 2018, pp. 376–379.

[13] J. G. Andrews, H. Claussen, M. Dohler, S. Rangan, and M. C. Reed, "Femtocells: Past, present, and future," *IEEE J. Sel. Areas Commun.*, vol. 30, no. 3, pp. 497–508, Apr. 2012.

[14] I. Ashraf, H. Claussen, and L. T. W. Ho, "Distributed radio coverage optimization in enterprise femtocell networks," in *Proc. IEEE Int. Conf. Commun.*, May 2010, pp. 1–6.

[15] S. R. Valizadeh and J. Abouei, "An adaptive distributed coverage optimization scheme in LTE enterprise femtocells," in *Proc. 22nd Iranian Conf. Electr. Eng. (ICEE)*, May 2014, pp. 1723–1728.

[16] H. Yuliana and A. Kurniawan, "Uplink power control for LTE femtocell based on overload indicator," in *Proc. Int. Symp. Electron. Smart Devices (ISESD)*, Nov. 2016, pp. 68–72.

[17] Y. Chen, J. Cheng, X. Wen, Z. Lu, and H. Shao, "An interference shaping based approach for energy saving of video applications," in *Proc. Int. Symp. Wireless Pers. Multimedia Commun. (WPMC)*, Sep. 2014, pp. 91–96.

[18] H. B. Jung and D. K. Kim, "Power control of femtocells based on max-min fairness in heterogeneous networks," *IEEE Commun. Lett.*, vol. 17, no. 7, pp. 1372–1375, Jul. 2013.

[19] S. E. Zegrar, A. E. Duranay, and H. Arslan, "Precoding based cross-tier interference mitigation in centralized-RAN," *IEEE Wireless Commun. Lett.*, vol. 10, no. 1, pp. 21–25, Jan. 2021.

[20] R. D. Ainul, H. Mahmudah, and A. Wijayanti, "Scheduling schemes of time and frequency resource allocation for interference coordination method based on user priority in LTE-femtocell," in *Proc. Int. Electron. Symp. (IES)*, Sep. 2015, pp. 178–182.

[21] K. Inage and T. Fujii, "Interference-adapted scheduling weight for small-cell in heterogeneous network," in *Proc. IEEE 24th Int. Symp. Pers., Indoor Mobile Radio Commun. (PIMRC Workshops)*, Sep. 2013, pp. 184–188.

[22] K. Yan, H.-C. Wu, S.-H. Fang, C. Wang, S. Li, and L. Zhang, "Indoor femtocell interference localization," *IEEE Trans. Wireless Commun.*, vol. 19, no. 8, pp. 5176–5187, Aug. 2020.

[23] S. Xing, P. Ghosal, K. Sandrasegaran, and A. Daeinabi, "System level simulation for femtocellular networks," in *Proc. Australas. Telecommun. Netw. Appl. Conf. (ATNAC)*, Nov. 2014, pp. 164–169.

[24] M. Cakir and A. Kalaycioglu, "Power adjustment based interference management in dense heterogeneous femtocell networks," in *Proc. 2nd Int. Conf. Comput. Commun. Syst. (ICCCS)*, Jul. 2017, pp. 133–137.

[25] J. Wang, J. Weitzen, O. Bayat, V. Sevindik, and M. Li, "Joint interference coordination approach in femtocell networks for QoS performance optimization," *Int. J. Commun. Syst.*, vol. 30, no. 12, Aug. 2017, Art. no. e3263, doi: 10.1002/dac.3263.

[26] F. Capozzi, G. Piro, L. A. Grieco, G. Boggia, and P. Camarda, "On accurate simulations of LTE femtocells using an open source simulator," *EURASIP J. Wireless Commun. Netw.*, vol. 2012, no. 1, p. 328, Dec. 2012. [Online]. Available: http://jwcn.eurasipjournals.com/content/2012/1/328

[27] R. R. Paulo, F. J. Velez, and G. Piro, "Performance evaluation and packet scheduling in HeNB deployments," in *Proc. IEEE 88th Veh. Technol. Conf. (VTC-Fall)*, Aug. 2018, pp. 1–6.

[28] *Simulation Assumptions and Parameters for FDD HeNB RF Requirements*, Standard 3GPP, R4-092042, 3rd Generation Partnership Project, Tech. Rep. Meeting #51, May 2009. [Online]. Available: https://www.3gpp.org/ftp7tsg_ran/WG4_Radio/TSGR4_51/Documents/R4_092042.zip

[29] H.-S. Jo, P. Xia, and J. G. Andrews, "Open, closed, and shared access femtocells in the downlink," *EURASIP J. Wireless Commun. Netw.*, vol. 2012, no. 1, p. 363, Dec. 2012, doi: 10.1186/1687-1499-2012-363.

[30] S. Wang, W. Guo, and T. O'Farrell, "Optimising femtocell placement in an interference limited network: Theory and simulation," in *Proc. IEEE Veh. Technol. Conf. (VTC Fall)*, Sep. 2012, pp. 1–6.

[31] C.-J. Liu, P. Huang, L. Xiao, and A.-H. Esfahanian, "Inter-femtocell interference identification and resource management," *IEEE Trans. Mobile Comput.*, vol. 19, no. 1, pp. 116–129, Jan. 2020.

[32] G. Piro, L. A. Grieco, G. Boggia, F. Capozzi, and P. Camarda, "Simulating LTE cellular systems: An open-source framework," *IEEE Trans. Veh. Technol.*, vol. 60, no. 2, pp. 498–513, Feb. 2011.

[33] R. R. Paulo and F. J. Velez, "A study on system capacity for HeNBs with different schedulers," in *Proc. Conf. Telecommun. - ConfTele*, Jun. 2019, pp. 25–28.

[34] J. Wu, B. Cheng, M. Wang, and J. Chen, "Energy-efficient bandwidth aggregation for delay-constrained video over heterogeneous wireless networks," *IEEE J. Sel. Areas Commun.*, vol. 35, no. 1, pp. 30–49, Jan. 2017.

[35] J. Wu, C. Yuen, B. Cheng, M. Wang, and J. Chen, "Energy-minimized multipath video transport to mobile devices in heterogeneous wireless networks," *IEEE J. Sel. Areas Commun.*, vol. 34, no. 5, pp. 1160–1178, May 2016.

[36] S. Sesia, I. Toufik, and M. Baker, *LTE, The UMTS Long Term Evolution: From Theory to Practice*, 2nd ed. Hoboken, NJ, USA: Wiley, 2011.

[37] H. A. M. Ramli, "A study on packet scheduling algorithms for healthcare contents over fifth generation (5G) mobile cellular network," *Int. J. Electron. Telecommun.*, vol. 66, no. 4, pp. 729–735, 2020.

[38] B. Abdelmula, H. S. Ali, M. Warip, M. N. Bin, O. Bi, and Y. Naimah, "Technical review of RRM for carrier aggregation in LTE-advanced," *J. Theor. Appl. Inf. Technol.*, vol. 91, pp. 397–410, Sep. 2016.

[39] G. Piro, L. A. Grieco, G. Boggia, R. Fortuna, and P. Camarda, "Two-level downlink scheduling for real-time multimedia services in LTE networks," *IEEE Trans. Multimedia*, vol. 13, no. 5, pp. 1052–1065, Oct. 2011.

[40] J. Jalali, A. Khalili, and H. Steendam, "Antenna selection and resource allocation in downlink MISO OFDMA femtocell networks," in *Proc. IEEE 91st Veh. Technol. Conf. (VTC-Spring)*, May 2020, pp. 1–6.

[41] J. Cao, T. Peng, X. Liu, W. Dong, R. Duan, Y. Yuan, W. Wang, and S. Cui, "Resource allocation for ultradense networks with machine-learning-based interference graph construction," *IEEE Internet Things J.*, vol. 7, no. 3, pp. 2137–2151, Mar. 2020.

[42] Y. Guo, C. Hu, T. Peng, H. Wang, and X. Guo, "Regression-based uplink interference identification and SINR prediction for 5G ultra-dense network," in *Proc. IEEE Int. Conf. Commun. (ICC)*, Jun. 2020, pp. 1–6.

[43] M. M. Nasralla, "A hybrid downlink scheduling approach for multi-traffic classes in LTE wireless systems," *IEEE Access*, vol. 8, pp. 82173–82186, 2020.

[44] M. M. Nasralla, N. Khan, and M. G. Martini, "Content-aware downlink scheduling for LTE wireless systems: A survey and performance comparison of key approaches," *Comput. Commun.*, vol. 130, pp. 78–100, Oct. 2018. [Online]. Available: http://www.sciencedirect.com/science/article/pii/S0140366418302020
[45] T. S. Rappaport, *Wireless Communications: Principles and Practice*, 2nd ed. Upper Saddle River, NJ, USA: Prentice-Hall, 2002.
[46] D. Robalo, "Planning and dynamic spectrum management in heterogeneous mobile networks with QoE optimization," Ph.D. dissertation, Dept. Electromech. Eng., Universidade da Beira Interior, Covilhã, Portugal, Aug. 2014. [Online]. Available: http://hdl.handle.net/10400.6/4033
[47] *Evolved Universal Terrestrial Radio Access (E-UTRA); Physical layer procedures (Release 15)*, Standard ETSI TS 136 213 V15.2.0, 3rd Generation Partnership Project, Tech. Rep. V15.0.0, Jun. 2014. [Online]. Available: http://www.3gpp.org/ftp/Specs/archive/36series/36.213/36213-f00.zip
[48] J. Habetha and J. Wiegert, "Network capacity optimisation—Part 1: Cellular radio networks," in *Proc. 10th Symp. Signal Theory*, Sep. 2001, pp. 125–132.
[49] J. Habetha and J. Wiegert, "Network capacity optimisation—Part 2: Multihop ad hoc radio networks," in *Proc. 10th Symp. Signal Theory*, Sep. 2001, pp. 133–140.
[50] H. Holma and A. Toskala, *WCDMA for UMTS—HSPA evolution and LTE*, 1st ed. West Sussex, U.K.: Wiley, 2007.
[51] K. Chen and J. de Marca, *Mobile WiMAX*. Hoboken, NJ, USA: Wiley, 2008. [Online]. Available: https://books.google.es/books?id=7TWzvbZkLMgC
[52] P. Kyösti, J. Meinilä, L. Hentilä, X. Zhao, T. Jämsä, C. Schneider, M. Narandzić, M. Milojević, A. Hong, J. Ylitalo, V. Holappa, M. Alatossava, R. Bultitude, Y. de Jong, and T. Rautiainen, "IST-4-027756 WINNER II D1.1.2 V1.2 WINNER II channel models," Inf. Soc. Technol., Berlin, Germany, Tech. Rep. D1.1.2 V1.2, Feb. 2008, p. 82. [Online]. Available: http://www.cept.org/files/1050/documents/winner2-final report.pdf
[53] K. Chen and J. de Marca, *Mobile WiMAX*. Hoboken, NJ, USA: Wiley, 2008, ch. Dimensioning cellular multi-hop WiMAX networks, pp. 203–234. [Online]. Available: https://books.google.es/books?id=7TWzvbZkLMgC
[54] X. Xu, G. Kutrolli, and R. Mathar, "Energy efficient power management for 4G heterogeneous cellular networks," in *Proc. IEEE 9th Int. Conf. Wireless Mobile Comput., Netw. Commun. (WiMob)*, Oct. 2013, pp. 231–238.
[55] O. Cabral, F. Meucci, A. Mihovska, F. J. Velez, N. R. Prasad, and R. Prasad, "Integrated common radio resource management with spectrum aggregation over non-contiguous frequency bands," *Wireless Pers. Commun.*, vol. 59, no. 3, pp. 499–523, Aug. 2011, doi: 10.1007/s11277-011-0242-6.
[56] M. Matsumoto and T. Nishimura, "Mersenne twister: A 623-dimensionally equidistributed uniform pseudo-random number generator," *ACM Trans. Model. Comput. Simul.*, vol. 8, no. 1, pp. 3–30, Jan. 1998, doi: 10.1145/272991.272995.
[57] S. Marsland, *Machine Learning: An Algorithmic Perspective*, 2nd ed. London, U.K.: Chapman & Hall, 2014.
[58] *International Standards Organization and International Electrotechnical Commission*, document ISO/IEC 9899:2011, Programming Languages–C, 1st ed. 11 West 42nd Street, New York, New York 1O036: American National Standards Institute (ANSI), Dec. 2011. [Online]. Available: http://www.open-std.org/jtc1/sc22/wg14/
[59] D. Shi, F. Tian, and S. Wu, "Energy efficiency optimization in heterogeneous networks based on deep reinforcement learning," in *Proc. IEEE Int. Conf. Commun. Workshops (ICC Workshops)*, Jun. 2020, pp. 1–6.
[60] F. J. Velez, T. Lages, and M. Veríssimo, "Redes sem Fios WiFi (IEEE 802.11) em Ambiente Hospitalar," in *Fórum Cyted-Iberoeka*. Lisbon, Portugal: Agência de Inovação, S.A., Sep. 2004.
[61] F. J. Velez, H. Santos, and T. Lages, "Redes sem Fios IEEE 802.11: Instalação, Configuração e Segurança," in *Proc. Conf. da Engenharia UBIEngenharias*, vol. 1, Nov. 2003, pp. 433–438.
[62] (2019). *V. T. Library*. [Online]. Available: http://trace.eas.asu.edu/tracemain.html
[63] R. R. Paulo. (2020). *LTE-SIM-RP*. [Online]. Available: https://github.com/RRP-IT/LTE-Sim-RP.git
[64] R. Basukala, H. A. M. Ramli, and K. Sandrasegaran, "Performance analysis of EXP/PF and M-LWDF in downlink 3GPP LTE system," in *Proc. 1st Asian Himalayas Int. Conf. Internet*, Nov. 2009, pp. 1–5.
[65] R. Kwan, C. Leung, and J. Zhang, "Proportional fair multiuser scheduling in LTE," *IEEE Signal Process. Lett.*, vol. 16, no. 6, pp. 461–464, Jun. 2009.
[66] E. Dahlman, S. Parkvall, J. Skold, and P. Beming, *3G Evolution, Second Edition: HSPA and LTE for Mobile Broadband*, 2nd ed. New York, NY, USA: Academic, 2008.
[67] S. Shakkottai and A. L. Stolyar, *Scheduling for Multiple Flows Sharing a Time-Varying Channel: The Exponential Rule*. Providence, RI, USA: American Mathematical Society Translations, Series, Nov. 2002, pp. 185–201.
[68] B. Sadiq, S. J. Baek, and G. de Veciana, "Delay-optimal opportunistic scheduling and approximations: The log rule," *IEEE/ACM Trans. Netw.*, vol. 19, no. 2, pp. 405–418, Apr. 2011.
[69] *Services and Service Capabilities (Release 15)*, Standard3GPP, TS 22.105, 3rd Generation Partnership Project, Tech. Rep. V15.0.0, Jul. 2018. [Online]. Available: https://www.3gpp.org/ftp/Specs/archive/25_series/25.892/25892-600.zip

RUI R. PAULO (Member, IEEE) received the Licenciatura and M.Sc. degrees in electromechanical engineering from the Universidade da Beira Interior (UBI), Covilhã, Portugal, in 2005 and 2008, respectively, where he is currently pursuing the Ph.D. degree in electrical and computer engineering. He has been serving as a Volunteer for the VTS Portugal Chapter, since 2006. He has also been with the Instituto de Telecomunicações, since 2006. His research interests include teletraffic engineering for wireless communications, radio resource management for small cell networks, and packet scheduling and network optimization in heterogeneous networks with femtocells.

FERNANDO J. VELEZ (Senior Member, IEEE) received the Licenciado, M.Sc., and Ph.D. degrees in electrical and computer engineering from the Instituto Superior Técnico, Technical University of Lisbon, in 1993, 1996, and 2001, respectively. Since 1995, he has been with the Department of Electromechanical Engineering, Universidade da Beira Interior, Covilhã, Portugal, where he is currently an Assistant Professor. He was an IEF Marie Curie Research Fellow with King's College London (KCL), from 2008 to 2009 (OPTIMOBILE IEF), and also a Marie Curie ERG Fellow with the Universidade da Beira Interior, from 2010 to March 2013 (PLANOPTI ERG). He is also a Senior Researcher with the Instituto de Telecomunicações. He is also the Coordinator of the Instituto de Telecomunicações Team in the Marie Skłodowska-Curie ITN Action (TeamUp5G), which began in 2019. He is or was part of the teams of several European and Portuguese research projects on mobile communications. He was the coordinator of six Portuguese projects. Recently, he was the Coordinator of CONQUEST (CMU/ECE/0030/2017), an exploratory project from Carnegie Mellon University (CMU), Portugal, a collaboration with the Department of Engineering and Public Policy, CMU. He has authored three books, 24 book chapters, 160 articles and communications in international journals and conferences, and 39 in national conferences. He is currently the IEEE VTS Region 8 (Europe, Middle East and Africa) Chapter Coordinator (nominated by VTS in 2010). He was the elected IEEE VTS Portugal Chapter Coordinator, from 2006 to 2014. He is also the Adjunct Coordinator of the Telecommunications Specialization of Ordem dos Engenheiros. He was the Coordinator of the WG2 (on Cognitive Radio/Software-Defined Radio Co-existence Studies) of COST IC0905 TERRA. His current research interests include cellular planning tools, traffic from mobility, wireless body sensor networks and wearable technologies, cross-layer design, spectrum sharing/aggregation, and the cost/revenue performance of advanced mobile communication systems.